IEEE Access
Multidisciplinary ⋮ Rapid Review ⋮ Open Access Journal

Received 12 July 2023, accepted 21 September 2023, date of publication 28 September 2023, date of current version 9 October 2023.

Digital Object Identifier 10.1109/ACCESS.2023.3320180

RESEARCH ARTICLE

Empirical Approaches for Improving Inertial Pedestrian Navigation: Approximating Gravitational Acceleration and Digitizing Heading Change Angles

JUNSEONG KIM, (Member, IEEE)
School of Electrical and Electronics Engineering, Chung-Ang University, Seoul 06974, South Korea
e-mail: junkim@cau.ac.kr

This work was supported by the Basic Science Research Program through the National Research Foundation of Korea (NRF) funded by the Ministry of Education under Grant NRF2021R1I1A205601811.

ABSTRACT Spatial mobility provides a rich context for human life, and the demand for indoor navigation and localization has increased. Pedestrian dead reckoning (PDR) is a viable solution thanks to its cost advantages and robustness to environmental changes. In this paper, we propose two generic ideas for improving inertial pedestrian navigation. One is about the estimation of gravitational acceleration and the other is about the estimation of heading change angles. Gravitational acceleration is dynamically extracted on the fly rather than assuming sensors to be fixed in a certain orientation. It can be used to estimate step lengths and heading change angles as a baseline. Also, heading change angles are digitized by combining the estimated gravitational acceleration with a simple threshold-based turn detection algorithm. Turns tend to occur across multiple steps and we separate turns from steps in walking. To demonstrate the effectiveness of the ideas a simple scheme, *steps-and-a-turn (SnT)*, is designed for inertial pedestrian navigation. In experiments using a complete daily route, we show that the estimation of gravitational acceleration is consistent and robust, and that the digitization of heading change angles is highly effective in typical building environments: the positioning error is about 1.2% of the total length of the experimental path. Various state-of-the-art schemes served on top of pure inertial pedestrian navigation are expected to benefit by utilizing the proposed ideas as basic building blocks.

INDEX TERMS Estimating gravitational accelerations, digitizing heading change angles, inertial navigation system, pedestrian dead reckoning, steps-and-a-turn.

I. INTRODUCTION

Enhancements in mobile devices and wireless communication technology demand location-based services in various fields including aerospace, robotics, healthcare, wellness, and entertainment to provide information on the surroundings for user convenience. In outdoor environments, GNSS (Global Navigation Satellite System) handles the requirements [1], [2]. For example, GPS (Global Positioning System) satellites orbiting the earth transmit signals such that GPS receivers can determine their locations on the earth with those signals. In indoor environments, however, it is difficult or impossible to provide services due to attenuations or blocking of satellite signals. Since people spend most of their time indoors (87% inside buildings and another 6% in automobiles) it is important to provide positioning information reliably in

The associate editor coordinating the review of this manuscript and approving it for publication was Andrea De Marcellis.

the environments [3]. Indoor navigation and localization are challenging tasks and an active topic for research and development.

Many different approaches for indoor navigation and localization have been proposed with their own strengths and weaknesses. There are methods relying on radio signals such as Wi-Fi, UWB, Bluetooth, etc. [4], [5], [6]. Using triangulation, it computes the distances between a mobile unit and an array of AP (access point) installed in buildings at known locations. Their initial cost is high because an infrastructure of AP is required. Also, these methods are sensitive to radio wave interference from walls, furniture, and other electronic devices. There are methods based on fingerprinting [4], [7], [8]. A map of various signal properties such as magnetic field or strength of communication signal is collected in a priori and compared to identify user's location. These methods have an advantage in terms of accuracy but are difficult to respond to environmental changes, which might be frequent due to mobile devices. Any environmental change means that a process of mapping, which is expensive and time-consuming, must be performed. There are methods without external references. Dead reckoning (DR) is a self-contained system, which uses inertial sensors [4], [9], [10], [11]. A user's location is estimated by reflecting the moving direction and distance from one's previously known position. Since no infrastructure or mapping process is required other than sensing devices to detect user's displacement, it has a great advantage in terms of cost and is robust against environmental changes. Drawbacks of DR approaches are noisy sensing data and cumulative errors over time. To complement errors there have been lots of efforts including map-aided approaches with domain-specific constraints or sensor fusions with additional data from magnetometers, GNSS systems [11], [12], [13], [14]. All those efforts are, however, based on pure inertial navigation systems.

As MEMS (Micro Electro-Mechanical Systems) inertial sensors become ubiquitous PDR (Pedestrian Dead Reckoning) systems are getting more interested [9], [15], [16], [17]. Their small-size, low-cost, low-power consumption make it easy to be embedded in smartphones and various wearable devices. However, MEMS-based sensors have, in general, large noise. In addition, pedestrians are all about humans that are not made up of a rigid body. Tedious and complicated calibration-based approaches do not work well. It is an area in which heuristics might be applicable for efficient solutions. In this paper, we propose two generic ideas for improving inertial pedestrian navigation. One is about the estimation of gravitational acceleration on the fly. Although the direction of gravity plays an essential role in PDR its practical estimations have not been actively pursued [10], [18], [19]. Instead, works in many literatures assume that sensing devices remain vertical during walking or demand that pedestrians hold sensing devices for a while with no movements. However, it is impractical to firmly fix sensing devices or is inconvenient to keep stationary period for pedestrians. We provide a practical and systematic procedure to estimate gravitational acceleration in real-time. By dynamically estimating gravitational acceleration pedestrians can be free in carrying sensing devices. The other idea is about the estimation of heading change angles. Heading estimation is a crucial part of PDR since it is a dominant factor in positioning accuracy. In many works of pedestrian navigation with a turn detection algorithm, pedestrians are considered walking straight when no turn is detected. The same considerations can be applied even when a turn is detected. We propose a method to digitize heading change angles by combining the estimated gravitational acceleration with a simple threshold-based turn detection algorithm. It is a simple but practical approach for pedestrian navigations, especially in typical buildings with straight corridors and limited directions.

To demonstrate the effectiveness of the ideas a simple scheme, called *steps-and-a-turn (SnT)*, is designed by combining basic building blocks of inertial pedestrian navigation. In experiments on a complete daily route, we show that the estimation of gravitational acceleration is consistent and robust, and that the digitization of heading change angles significantly reduces errors in pedestrian navigation. We expect that the proposed ideas, as basic building blocks, will improve existing state-of-the-art schemes including sensor fusions or map-aided techniques as they are served on top of pure inertial pedestrian navigation.

The remainder of this paper is organized as follows. In Section II we describe the algorithm for estimating gravitational acceleration and the details of digitizing heading change angles. Also, a brief description of the SnT scheme is presented. Section III provides a comprehensive evaluation and analysis of the experiments and results. Finally, Section IV summarizes our results and conclusions.

II. MEMS BASED INERTIAL PEDESTRIAN NAVIGATION

DR is a self-contained navigation technique commonly used in the past for ships, aircraft, and missiles. It estimates a relative location rather than an absolute one by using inertial measurement units (IMU) - a combination of accelerometers and gyroscopes. Current position (x_n, y_n) is determined by updating its known previous location (x_{n-1}, y_{n-1}) based on the displacement of traveled distance d and directional change θ.

$$(x_n, y_n) = (x_{n-1} + d \cdot cos\theta, y_{n-1} + d \cdot sin\theta) \quad (1)$$

In the context of PDR, a modified form of DR, two reference coordinates, namely navigation (N) frame and body (B) frame, are utilized [10], [18], [20]. N-frame is the coordinate for indicating a pedestrian's position according to his or her mobility. B-frame refers to the coordinate where sensors are attached for measurements. Since B-frame and N-frame, in general, do not coincide with each other, a coordinate transformation needs to be performed. For example, a vector $\overrightarrow{V_b}$ on B-frame can be transformed to a vector $\overrightarrow{V_n}$ on N-frame as shown in Figure 1. It shows the Euler rotation sequence of Z-Y-X denoting an initial rotation about the Z-axis by ψ, then

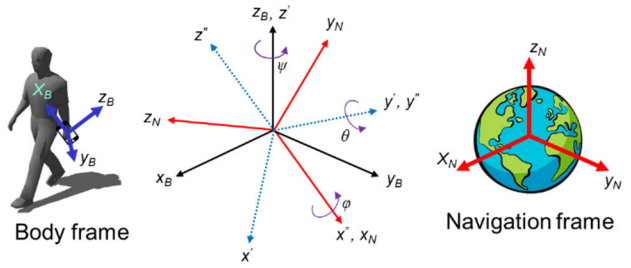

FIGURE 1. The coordinate transformation between B-frame and N-frame: the Euler rotation sequence of Z-Y-X.

about the rotated Y-axis (denoted y′) by θ, and finally about the twice-rotated X-axis (denoted x″) by $\emptyset$.

$$\overrightarrow{V_n} = R\overrightarrow{V_b}$$
$$R = \begin{bmatrix} 1 & 0 & 0 \\ 0 & cos\emptyset & sin\emptyset \\ 0 & -sin\emptyset & cos\emptyset \end{bmatrix} \begin{bmatrix} cos\theta & 0 & -sin\theta \\ 0 & 1 & 0 \\ sin\theta & 0 & cos\theta \end{bmatrix} \times \begin{bmatrix} cos\psi & sin\psi & 0 \\ -sin\psi & cos\psi & 0 \\ 0 & 0 & 1 \end{bmatrix} \quad (2)$$

In a typical INS (Inertial Navigation System), the tri-axial accelerometer signals on N-frame are double integrated for traveled distance and the gyroscopes signals on N-frame are single integrated for directional change [4], [9], [21]. In the process it is necessary to subtract acceleration due to gravity. A critical drawback of this approach is that errors are rapidly accumulated over time.

SHS (Step and Heading System) is an alternative approach for pedestrian navigation. It indirectly calculates traveled distance based on pedestrian's walking model called *gait cycle* [11], [22], [23]. It counts number of steps from measured signals and multiplied by step length for traveled distance. Since number of steps is proportional to time, the accumulated error can be reduced. In addition, a noise margin of sensors can be secured in the conversion process. A typical SHS uses the same heading estimation as INS.

A. ESTIMATING GRAVITATIONAL ACCELERATION

Accelerometers measure linear accelerations caused by a pedestrian's motion. While tri-axial accelerometer signals are time-varying there exists the static gravitational acceleration within them [10], [18].

$$\overrightarrow{acc_b} = \overrightarrow{f_b} + \overrightarrow{g_b} \quad (3)$$

where $\overrightarrow{acc_b} = (acc_{b\_x}, acc_{b\_y}, acc_{b\_z})$ is the vector made up of the accelerometer measurements on B-frame, $\overrightarrow{f_b}$ is the dynamic component by a pedestrian's specific motion and $\overrightarrow{g_b}$ is the static component by gravitational accelerations. Also, accelerometer measurements can be decomposed into its vertical component $\overrightarrow{acc_v}$ and horizontal component $\overrightarrow{acc_h}$.

$$\overrightarrow{acc_b} = \overrightarrow{acc_v} + \overrightarrow{acc_h} \quad (4)$$

Since the gravitational acceleration $\overrightarrow{g_b}$ is apparently parallel to the vertical component on N-frame, for a given measured signal $\overrightarrow{acc_b}$, we have the vertical component $\overrightarrow{acc_v} = \overrightarrow{acc_b} \cdot \overrightarrow{g_b}$ by vector dot product and the horizontal component $\overrightarrow{acc_h} = \overrightarrow{acc_b} - \overrightarrow{acc_v}$ by vector subtraction. Then, the horizontal components $\overrightarrow{acc_h}$ can directly be used for the calculation of traveled distance d without coordinate transformations. Also, the vertical component $\overrightarrow{acc_v}$ can be used for the estimation of directional change θ.

We propose a practical procedure to extract the gravitational acceleration $\overrightarrow{g_b}$ from the measurements $\overrightarrow{acc_b}$ on B-frame. Ideally, when there is no movement, the dynamic component $\overrightarrow{f_b}$ will be zero being $\overrightarrow{acc_b} = \overrightarrow{g_b}$, of which magnitude approaches 9.81 m/s^2. Practically, when $\overrightarrow{f_b}$ is minimum, $\overrightarrow{acc_b}$ is likely to be dominated by gravitational acceleration being $\overrightarrow{acc_b} \approx \overrightarrow{g_b}$. We can approximate the gravitational acceleration $\overrightarrow{g_b}$ by capturing the instantaneous stationary moment of pedestrians' walking such as

1. Measured acceleration signals are segmented, as in SHS, by steps. Let's say there are K_{step} measured samples within a step.
2. Calculate magnitude of acceleration $|\overrightarrow{acc_b}|$ for each K_{step} measured samples.
$$|\overrightarrow{acc_b}| = \sqrt{acc_{b\_x}^2 + acc_{b\_y}^2 + acc_{b\_z}^2} \quad (5)$$
3. Choose a measured signal $\overrightarrow{acc_b}$ among K_{step} measured samples as a gravitational acceleration-possible $\overrightarrow{g_{b,guess}}$ based on the value of $|\overrightarrow{acc_b}|$. It corresponds to the moment at which the pedestrian appears to be barely moved within a step.
4. The gravitational acceleration $\overrightarrow{g_b}$ is estimated dynamically by taking the moving average of gravitational acceleration-possibles $\overrightarrow{g_{b,guess}}$ of its previous N steps:
$$\overrightarrow{g_b[n]} \approx \frac{1}{N} \sum_{i=0}^{N-1} \overrightarrow{g_{b,guess}[n-i]} \quad (6)$$

For the gravitational acceleration-possible $\overrightarrow{g_{b,guess}}$ we consider the following four candidates among K_{step} measured samples within a step.

- Maximum magnitude $\overrightarrow{g_{b,Peak}}$: the measured value $\overrightarrow{acc_b}$ at the point when the magnitude $|\overrightarrow{acc_b}|$ is maximum.
- Minimum magnitude $\overrightarrow{g_{b,Valley}}$: the measured value $\overrightarrow{acc_b}$ at the point when the magnitude $|\overrightarrow{acc_b}|$ is minimum.
- Minimum difference in magnitude $\overrightarrow{g_{b,MinDiff}}$: the measured value $\overrightarrow{acc_b}$ at the point when the magnitude difference between two consecutive acceleration signals is minimum.
- Arithmetic mean $\overrightarrow{g_{b,AvgPV}}$: the average of $\overrightarrow{g_{b,Peak}}$ and $\overrightarrow{g_{b,Valley}}$.

B. ESTIMATING HEADING CHANGE ANGLES

Heading change estimation is the most crucial process in PDR applications since a heading change angle is a dominant factor in navigation accuracy [10], [19]. We present a practical procedure to estimate heading change angle θ relying both

on the estimated gravitational acceleration $\overrightarrow{g_b}$ and on a simple threshold-based turn detection algorithm.

Gyroscopes measure angular velocity and let $\overrightarrow{gyro_b} = (gyro_{b\_x}, gyro_{b\_y}, gyro_{b\_z})$ be the vector made up of the gyroscope measurements on B-frame. We define a *turn* as a pedestrian's single monotonic motion that does not change its direction in the middle. To reduce any effects of the way to carry a sensing device, the magnitude of angular velocity data collected from three axes perpendicular to each other is considered.

$$|\overrightarrow{gyro_b}| = \sqrt{gyro_{b\_x}^2 + gyro_{b\_y}^2 + gyro_{b\_z}^2} \tag{7}$$

There is a single threshold Th_{gyro} such that heading change estimation can be performed only when a turn is detected. A turn begins when the magnitude of the angular velocity $|\overrightarrow{gyro_b}|$ crosses upward the threshold Th_{gyro}. Then, a peak during the turn is retrieved. There might be multiple peaks within a turn and we consider the largest as a peak. A turn is finalized when the magnitude of the angular velocity $|\overrightarrow{gyro_b}|$ crosses downward the threshold Th_{gyro}. The value of Th_{gyro} is set high enough to be sensitive to pedestrian's heading changes but not to other causes of rotation.

Figure 2 shows the concept of turn detections. The line graph is the magnitude of angular velocity data $|\overrightarrow{gyro_b}|$ on the primary y-axis and the impulse graph represents different phases of turn detection on the secondary y-axis: the beginning, the peak, and the end. We define *turn period* as $t_{turn} = t_{2Peak} + t_{2End}$. The turn period and amplitude are reflected in turn detection algorithm such that only peaks with sufficient amplitude and period are considered valid turns. We empirically determine the minimum amplitude of a valid peak and the average period of a valid turn through preliminary experiments.

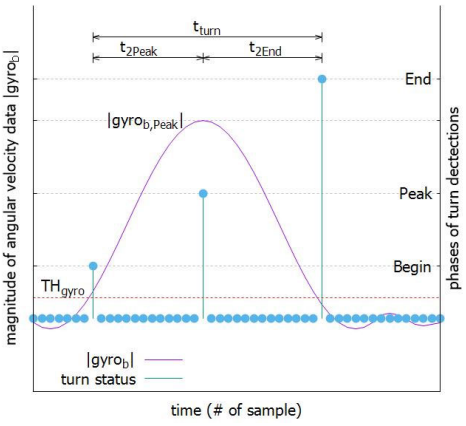

FIGURE 2. The concept of turn detections: turn period and amplitude.

Let's say there are K_{turn} samples of gyroscope measurement for a turn detected. According to Euler's rotation theorem, any 3D rotation can be specified by axis-angle representation [24], [25]. That is, each of the K_{turn} samples from the turn detection represents a rotation angle $|\overrightarrow{gyro_b}|\,\Delta t$ around the axis $\overrightarrow{gyro_b}$ where Δt is the sampling period of the gyroscope. Since pedestrians move horizontally, we expect that the rotation axis $\overrightarrow{gyro_b}$ is parallel to the gravitational acceleration vector $\overrightarrow{g_b}$. However, that is not true in general because measured signals include rotation behaviors other than pedestrian's heading change. Instead, we project the angular velocity vector $\overrightarrow{gyro_b}$ to the gravitational acceleration $\overrightarrow{g_b}$.

$$\overrightarrow{\omega_b} = \frac{\overrightarrow{gyro_b} \cdot \overrightarrow{g_b}}{|\overrightarrow{g_b}|} \tag{8}$$

The projected angular velocity vector $\overrightarrow{\omega_b}$ represents a rotation around the axis of the gravitational acceleration $\overrightarrow{g_b}$ by the angle $|\overrightarrow{\omega_b}|\,\Delta t$. The heading change angle θ can be approximated by considering all the K_{turn} samples during the turn.

$$\theta \approx \alpha * \left(\sum_{i=0}^{K_{turn}-1} \left| \overrightarrow{\omega_b\,[n-i]} \right| \Delta t \right) + \theta_{bias} \tag{9}$$

where α is a scale factor and θ_{bias} is a bias to complement the turn detection algorithm. It is a threshold-based one and detections are naturally lagged by several samples from the actual beginning of a turn. Also, there exists leftovers after finalizing a turn by several samples. It can be complemented by a small constant since they correspond to the head and tail in the magnitude of angular velocity data. In this study, we set α to 1 and θ_{bias} to 0 for simplicity.

With MEMS-based sensors, however, we easily find that the estimated heading change angle θ is not accurate. We also understand that walking is restricted in an indoor environment. A typical man-made building has straight corridors and fewer than eight directions, with four being dominant. Therefore, it is practical to assume that turns in an indoor environment occur only to some extent by digitizing the heading change angle. In fact, in many works of pedestrian navigation, a pedestrian is assumed to be walking straight if no turn is detected. We extend the same considerations even when a turn is detected. The problem is the resolution of the unit angle for the digitization. Though it is desirable to have a fine resolution, in this study, a coarse resolution of 45° is considered for demonstration purposes. This can be done by separating turns from steps in walking with the turn detection algorithm. That is, by considering a turn as a whole, the estimated heading change angle θ becomes eminent enough to be digitized. Otherwise, the heading change angle θ is easily amortized into steps blurry because a turn tends to occur over multiple steps. In addition, we can manage the resolution dynamically by reflecting the structure of a building in map-aided approaches or by utilizing additional data from magnetometers in sensor fusion approaches.

C. INERTIAL PEDESTRIAN NAVIGATION

To demonstrate how to utilize the proposed ideas for PDR applications we design a simple scheme, which belongs to the class of SHS, by combining basic building blocks of pedestrian navigation. Some are from the proposed ideas and others

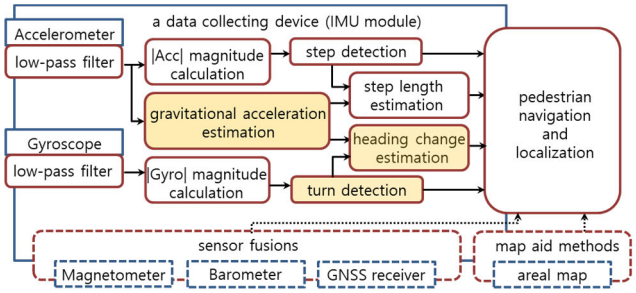

FIGURE 3. The structure of an inertial pedestrian navigation system.

from existing algorithms. We call this scheme *steps-and-a-turn(SnT)* to emphasize the fact that a turn occurs across multiple steps. Figure 3 shows the structure of an inertial pedestrian navigation system. The blocks of a straight line are utilized in this study and the ones of a dotted line including sensor fusions are for extensions in near future. Each block can be substituted with any well-modeled algorithm for obtaining a pedestrian's complete trajectory. We want algorithms that are simple and practical with low computational complexity. The shaded blocks of gravitational acceleration estimation, the turn detection, and the heading change estimation are based on the proposed ideas in this study.

Many works have been done for step detection including peak detection, zero-crossing, and correlation techniques [23], [26], [27]. The key idea is the recognition of repeated patterns in measured data. In this study, we borrow a threshold-based step detection algorithm and slightly modify it to reflect both the step period and amplitude. Accelerometers are used and, as with gyroscopes, the magnitude of acceleration data $\left|\overrightarrow{acc_b}\right|$ is considered. There is an upper threshold Th_{accH} and a lower threshold Th_{accL} such that step counting can only be performed when a pedestrian is walking. A step begins when the magnitude of acceleration $\left|\overrightarrow{acc_b}\right|$ crosses the upper threshold Th_{accH}. Then, a pair of peak-and-valley during the step is retrieved. It corresponds to a consecutive detection of a swing phase followed by a stance phase in the human gait cycle. A gait cycle consists of a stance phase (60∼62%) when the foot of interest touches the ground and a swing phase (38∼40%) when the foot of interest is in the air [22]. Both feet are on the ground during the first and last 10∼12% of the stance phase. Depending on pedestrians' behavior there might be multiple peaks or valleys within a step. We consider the largest as a peak and the smallest as a valley. Once a pair of peak-and-valley is found then the next crossing of the lower threshold Th_{accL} finalizes its current step. The very next crossing of the upper threshold Th_{accH} after the crossing of Th_{accL} represents the beginning of a new step. As with turn detection, only pairs of peak-and-valley with sufficient amplitude and period are considered valid steps to prevent missing or fake step occurrences. We empirically determine the minimum amplitude of a valid peak, the maximum amplitude of a valid valley, and the average period of a valid step through preliminary experiments.

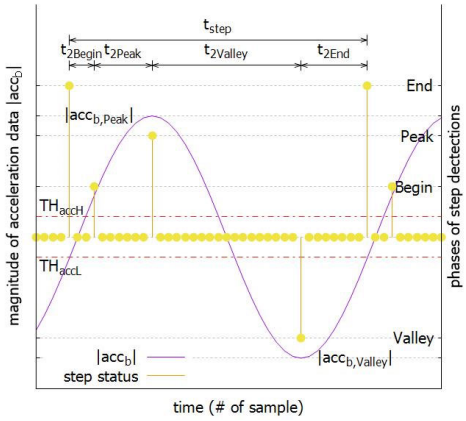

FIGURE 4. The concept of step detections: step period and amplitude.

Figure 4 shows the concept of step detections. The line graph is the magnitude of acceleration data $\left|\overrightarrow{acc_b}\right|$ on the primary y-axis. The impulse graph represents different phases of step detection on the secondary y-axis: the beginning, the peak, the valley, and the end. By separating the beginning of a step from the end of its previous step we can clearly identify a pedestrian's movement according to the gait cycle. We define *step period* from the end of its previous step to the end of current step such that $t_{step} = t_{2Begin} + t_{2Peak} + t_{2Valley} + t_{2End}$. It is assumed that $t_{2Begin} = 0$ for the first step of a walk segment.

Traveled distance d is estimated by multiplying step count and step length. Though step length depends on various factors including pedestrian's height, walking speed, acceleration variance, etc. it is well modelled in many literatures [11], [23], [27], [28]. Also, different step length model does not affect the positioning accuracy severely in PDR applications. In this study, we use, for our convenience, the empirical model by Weinberg [29].

$$StepLength \approx k\sqrt[4]{\left|acc_{v,max}\right| - \left|acc_{v,min}\right|} \tag{10}$$

where $\left|acc_{v,max}\right|$ and $\left|acc_{v,min}\right|$ are the maximum and the minimum of vertical acceleration components for each step and k is a proportional factor that needs to be calibrated for each pedestrian. This model is easy to implement, and we can have $\overrightarrow{acc_{v,max}}$ and $\overrightarrow{acc_{v,min}}$ during the step detection process as well.

III. EXPERIMENTS AND RESULTS

To control the whole process of experiments from data collection to pedestrian navigation we design a device with the Atmega328P microcontroller and the GY-89 IMU module using an I2C interconnection. GY-89 is a typical low-cost MEMS-based inertial sensor module and contains an LSM303D accelerometer and an L3GD20 gyroscope of STMicroelectronics [30], [31]. The measurement range of L3GD20 is configured by ±250 dps, and that of LSM303D by ±2 g. This device gathers raw sensing data every 50 ms (20 Hz) and applies 2nd order Butterworth low-pass filter

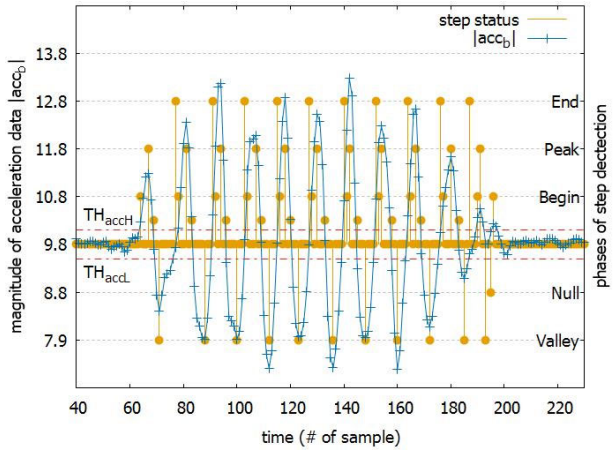

FIGURE 5. Step detections for a walk segment of 10 steps.

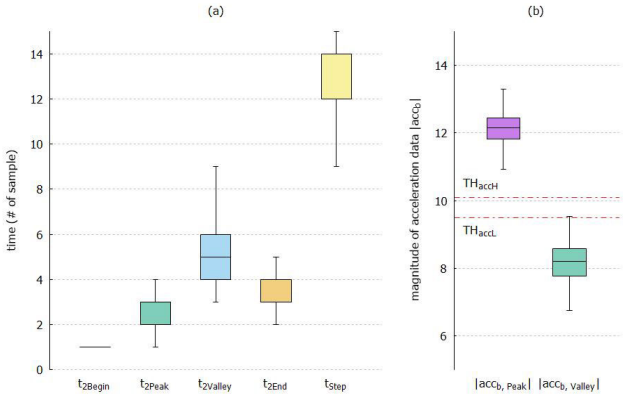

FIGURE 6. Extra contexts of the step detection: (a) step period and (b) step amplitude.

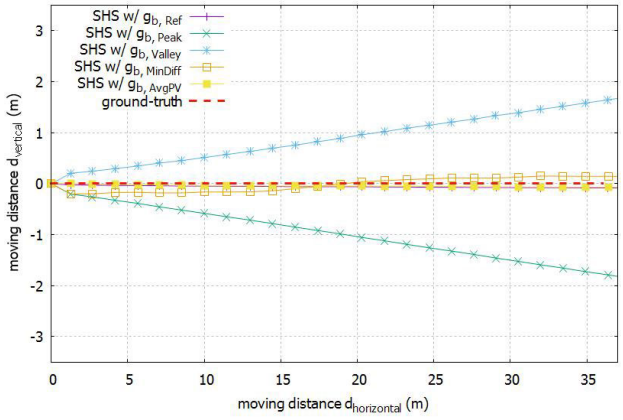

FIGURE 7. Moving distance of a typical SHS with various gravitational acceleration-possible $\overrightarrow{g_{b,guess}}$.

to manage noise from the low-quality MEMS sensors. The cutoff frequency is set to 3.5 Hz in consideration of typical pedestrians' walking frequency of 1.48 to 2.61 Hz [32]. A uSD module with UART interconnect is used for manipulation of the collected data. Four participants are involved in the experiment. They held the data collecting device with one hand and keep his or her attitude while walking. Participants are briefed on the experiments and asked to walk naturally without intentional acceleration or deceleration. Walking backward or sideward is not allowed. It is assumed that participants' initial orientation is known in advance.

A. STEP DETECTION AND STEP LENGTH ESTIMATION

We conduct the experiments in a corridor of 36.0 m in length and 3.0 m in width. Participants walk straight 10 steps and pause for a while then repeat. At the beginning and end of a walk segment, both feet are set parallel. That is, for the walk segment, there is an extra (the 11^{th}) step that does not contribute to any advance in moving distance. Since step count is directly related to moving distance, the last step would rather not be counted.

Figure 5 shows a result of the proposed step detection for a walk segment. The line graph represents the magnitude of acceleration data $|\overrightarrow{acc_b}|$ and the impulse graph represents different phases of step detection. It also shows the upper threshold $Th_{accH} = 10.1$ and the lower threshold $Th_{accL} = 9.5$ for convenience. As expected, the acceleration data has a clear biphasic pattern during walking. Experimental results show a detection accuracy of 99.6%. It successfully detects steps as do existing methods in many literatures. The contexts of step detection, however, are much richer by identifying different phases of a step.

Figure 6 shows the extra contexts of step period and amplitude in boxplots. Step take a 12.8 sampling period on average, which is 0.64 sec in this experiment. A swing phase roughly corresponds to the duration of $(t_{2Peak} + t_{2Valley})$ and the double limb support of a stance phase corresponds to $(t_{2Begin} + t_{2End})$. We use these data in the step detection algorithm. Only peak-and-valley pairs, whose amplitudes $|\overrightarrow{acc_b}|$ are within the 1.5 IQR (Interquartile Range), are considered valid steps excluding outliers. That is, the peaks whose amplitude $|\overrightarrow{acc_{b,Peak}}|$ larger than Q1-1.5 IQR and the valley whose amplitude $|\overrightarrow{acc_{b,Valley}}|$ smaller than Q3+1.5 IQR are valid. In Figure 5, we can see that the 11^{th} step of a walk segment is nullified using the extra contexts of step detection. It cannot be expected if we use a simple peak detection algorithm, which counts a step at an early stage of step activity. A missing or a fake step count tends to occur at the beginning or end of a walk segment. The extra contexts can be used for various pedestrian-related problems since people have different physical characteristics including the disabled.

We repeat the experiments, but participants walk without being disturbed along the same corridor. At the beginning and end of a walk, both feet are set parallel. The Weinberg model is used to estimate step length. Gravitational acceleration $\overrightarrow{g_b}$ in equation (6) is provided dynamically by taking the moving average of the previous 5 steps (N=5). In addition, participants are asked to remain stationary for a few seconds before each trial so that we can take the average of the measured acceleration $\overrightarrow{acc_b}$ during the stationary interval as a reference for gravitational acceleration $\overrightarrow{g_{b,Ref}}$.

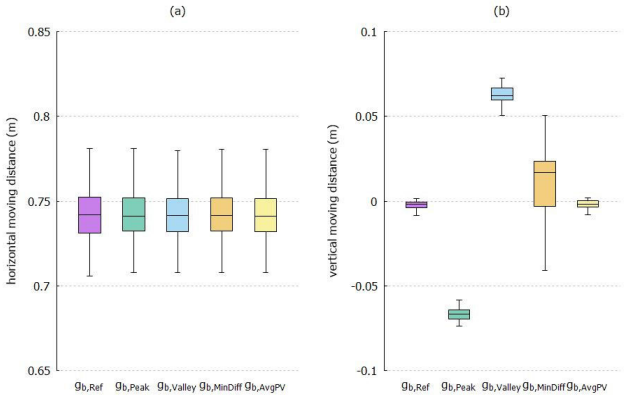

FIGURE 8. Per-step moving distance of a typical SHS with various gravitational acceleration-possible $\overrightarrow{g_{b,guess}}$: (a) horizontal moving distance and (b) vertical moving distance.

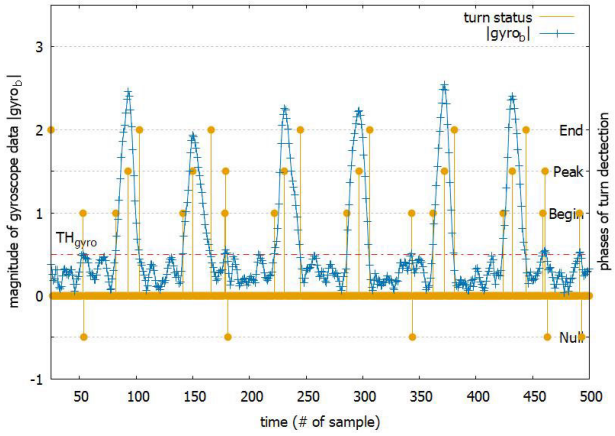

FIGURE 9. Turn detections for a walk in a zig-zag fashion with 90° turns.

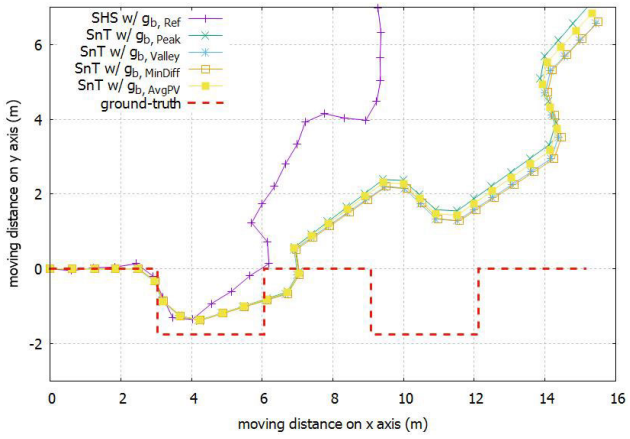

FIGURE 10. Horizontal trajectory on the xy-plane for SHS with $\overrightarrow{g_{b,Ref}}$ and SnT with various gravitational acceleration-possible $\overrightarrow{g_{b,guess}}$.

Figure 7 shows a result for the moving distance of a typical SHS with various gravitational acceleration-possible $\overrightarrow{g_{b,guess}}$. The graph represents the navigation trajectory on the xz-plane of N-frame. It also includes the ground truth of 36.0 m. We ignore any directional changes if any. We set the proportional constant k of the Weinberg model properly for each participant: the k is set between 0.478 and 0.508. This is the only parameter to be personalized in the experiments. The participant's data is provided on Table 2 in Appendix. From the graph, we can see that, with different gravitational acceleration-possible $\overrightarrow{g_{b,guess}}$ pedestrians move similarly horizontally but differently vertically. Note that the experiment is carried out on a non-tilted hallway.

Figure 8 is the moving distance per step in boxplots. We can see that pedestrians move forward horizontally by about 0.73 m on every step regardless of the gravitational acceleration-possible $\overrightarrow{g_{b,guess}}$. Also, from the graph, we can figure out the cause of the difference in vertical movements with the different gravitational acceleration-possible $\overrightarrow{g_{b,guess}}$. Pedestrians move downhill or uphill at about 0.06 m on every step with $\overrightarrow{g_{b,Peak}}$ or $\overrightarrow{g_{b,Valley}}$, respectively. It happens because $\overrightarrow{g_{b,Peak}}$ is chosen right after a maximum of $|\overrightarrow{acc_b}|$, which is likely downward. Similarly, $\overrightarrow{g_{b,Valley}}$ is chosen right after a minimum of $|\overrightarrow{acc_b}|$, which is likely upward. Errors are accumulated over the number of steps. With $\overrightarrow{g_{b,MinDiff}}$ pedestrians appear to move up and down slightly. We can say that the minimum difference point of $|\overrightarrow{acc_b}|$ within a step is inconsistent. The $\overrightarrow{g_{b,AvgPV}}$ is most stable with respect to vertical movements providing a trajectory comparable to that with $\overrightarrow{g_{b,Ref}}$. We can expect the gravitational acceleration-possible of $\overrightarrow{g_{b,AvgPV}}$ to perform well for pedestrian navigation.

B. TURN DETECTION AND HEADING CHANGE ESTIMATION

We run the experiments in the same corridor but participants walk in a zig-zag fashion with 90° turns. Figure 9 shows a result of the proposed turn detection. The line graph represents the magnitude of angular velocity $|\overrightarrow{gyro_b}|$ and the impulse graph represents different phases of turn detection. It also shows the threshold $Th_{gyro} = 0.5$ for convenience. The magnitude of angular velocity $|\overrightarrow{gyro_b}|$ at peaks is so large that we can easily tell a 90° turn. Also, we can see that the angular velocity data fluctuate irregularly even when pedestrians walk straight. Turns are 100% detected throughout the experiments.

Figure 10 shows the corresponding navigation trajectory on the horizontal xy-plane of N-frame. It includes the trajectory of a typical SHS using $\overrightarrow{g_{b,Ref}}$ and that of SnT using various $\overrightarrow{g_{b,guess}}$. It also provides the ground truth consisting of 4 left turns and 4 right turns as an expected trajectory. We can see that the trajectory of SHS deviates rapidly as steps go on. When pedestrians walk straight the heading change angle is expected to be zero. However, the estimation of heading change angle is off by some small values at each step being continuously accumulated. In SnT, the estimated heading change angle is deployed only when a turn is detected, which eliminates the slightly deviated stepwise drifts. There are flat lines in the trajectory resulting from the turn detection algorithm. Using different gravitational acceleration-possible

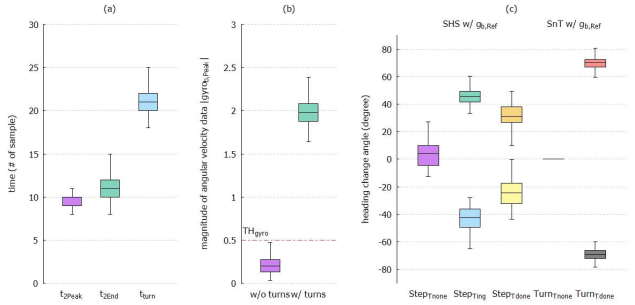

FIGURE 11. Extra contexts of turn detection: (a) turn period (b) turn amplitude and (c) heading change angles for SHS and SnT with $\overrightarrow{g_{b,Ref}}$.

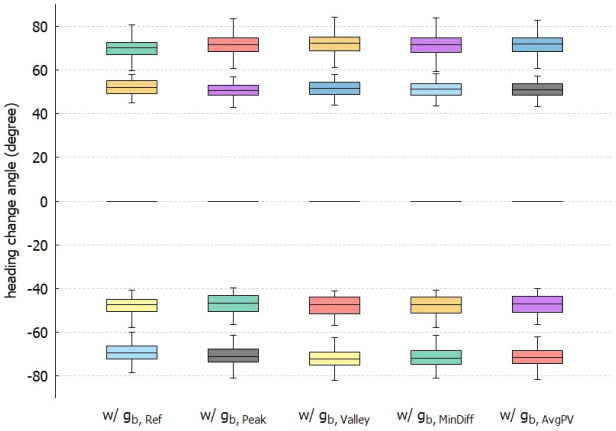

FIGURE 12. Per-turn heading change angles of SnT with various gravitational acceleration-possible $\overrightarrow{g_{b,guess}}$.

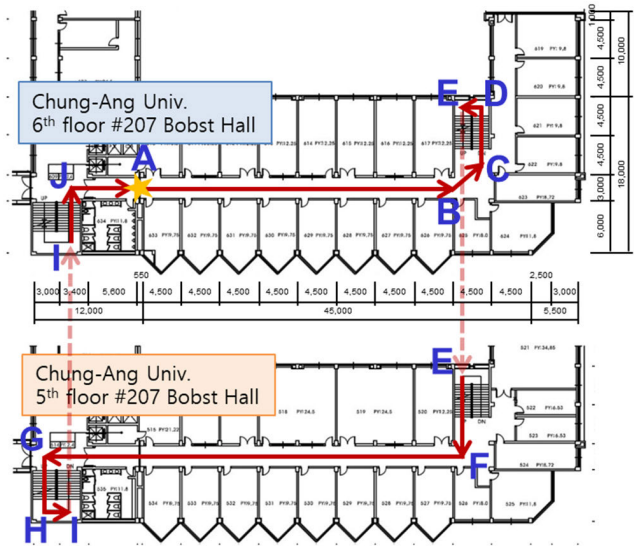

FIGURE 13. The experimental path in #207 engineering building, Chung-Ang University.

$\overrightarrow{g_{b,guess}}$ is not critical concerning the estimation of heading change angle.

Figure 11 shows the extra contexts of 90° turns with respect to its period, amplitude, and estimated heading change angle. We can confirm that at peaks the magnitude of angular velocity $|\overrightarrow{gyro_{b,Peak}}|$ is eminent. Also, it shows that a 90° turn takes around 21.2 sample period on average, which means that two or three steps are involved for a single turn. On that extension, we classify steps into three types: a step in straight walking $Step_{Tnone}$, a step with a turn in progress $Step_{Ting}$, and a step with a finalized turn $Step_{Tdone}$. Figure 11 (c) shows the estimated heading change angles of a typical SHS and SnT with $\overrightarrow{g_{b,Ref}}$. Note that the values of SHS are per step of different types while the values of SnT are per turn. Positive angles correspond to left turns and negative to right in this experiment. We can compare $\text{Step}_{\text{Tnone}}$ of SHS with $\text{Turn}_{\text{Tnone}}$ of SnT. Pedestrians sway by about 2.9° with each step even when they walk straight. In SHS, sway angle directly contributes to deviating pedestrians' trajectory. In SnT, however, since a turn is not detected during the period sway angle can be ignored. Similarly, we can compare $\text{Step}_{\text{Ting}}$ and $\text{Step}_{\text{Tdone}}$ of SHS with $\text{Turn}_{\text{Tdone}}$ of SnT. Because a turn can begin or end in the middle of a step $\text{Turn}_{\text{Tdone}} \leq \text{Step}_{\text{Ting}} + \text{Step}_{\text{Tdone}}$. In SnT, the angle of 90° for a single turn is counted as a whole such that it can be clearly distinguished, but in SHS, it is amortized in several steps blurry.

With SnT, we can imagine digitized heading change angles. We run the same experiments but with 45° turns. Figure 12 shows the estimated heading change angles of SnT with various gravitational acceleration-possible $\overrightarrow{g_{b,guess}}$. Each column has five boxplots in the order from the top: 90° and 45° left turn, straight walk, 45° and 90° right turn. We can see that there are only marginal differences in the estimated heading change angle using different $\overrightarrow{g_{b,guess}}$. It can be said that the direction, left or right, of turns can be completely distinguished. Also, by considering the 1.5 IQR we can identify the heading change angle between 90°, 45°, 0°, −45°, and −90°. None of the whiskers in the boxplot are overlapped each other: $\overrightarrow{g_{b,AvgPV}}$ seems to have noise margins for both left and right turns. It is desirable to have a fine resolution at heading change angles but digitizing by 45° is practical. Typical buildings consist of straight corridors and a limited number of pathways, with four being dominant. We will call this scheme *digitized SnT*.

C. PEDESTRIAN NAVIGATION

To evaluate the effectiveness of the proposed ideas a set of experiments is performed with a complete daily route involving a sequence of walking and making turns. Figure 13 is the path we used in the experiments: the 6th and the 5th floor of #207 engineering building at Chung-Ang University, Seoul. It starts at 'A', proceeds in alphabetical order, and returns to the starting point 'A' again consisting of corridors and stairs with a total length of 157.5m including 7 left turns and 2 right turns. The turns at 'B' and 'C' are 45° and the others are 90°. The path can be divided into four sections. In sections 'J-A-B-C' and 'F-G' pedestrians move horizontally. They correspond to the corridor on the 6th and

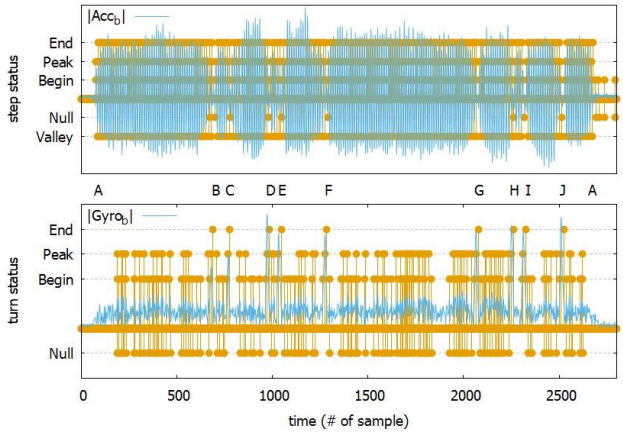

FIGURE 14. Step detection and turn detection along the experimental path.

the 5th floor, respectively. In sections 'C-D-E-F' and 'G-H-I-J' pedestrians move vertically as well as horizontally. They include stairs between the floors. Subsections 'D-E' and 'H-I' indicate landings in the middle of stairs.

Figure 14 shows a result of the steps and turns detected while a participant moves along the experimental path. It provides, for convenience, the same label as in Figure 13 for the location of turns on the x-axis. We can see that all 9 turns are successfully detected. Also, the step detection counts 207 while the participant walks 208 steps, which results in detection accuracy of 99.52%.

Figure 15 shows the corresponding navigation trajectory both on the horizontal xy-plane and on the vertical xz-plane of N-frame. It includes the trajectory of a typical INS and SHS with $\overrightarrow{g_{b,Ref}}$ and the trajectory of SnT and digitized SnT with $\overrightarrow{g_{b,AvgPV}}$. From the trajectory on the xz-plane, we can see that none of the methods comply with the vertical movement. PDR itself is about 2D navigation and the change in pedestrians' acceleration is very small compared to the magnitude of gravity. From the trajectory on the horizontal xy-plane, we can see the trajectory of digitized SnT follows the ground truth. Typical INS and SHS deviate from the ground truth in the early stages of walking. We can easily see the impact of accumulated errors on navigation over time. SHS just utilizes a realistic model in step length over INS. The trajectory deviation of SnT is delayed until a couple of turns occur. With a turn detection it works for short-term navigation. This corresponds to a digitization of heading change angles only when walking straight.

In order to quantitatively compare the effectiveness of the proposed ideas we use *synchronized Euclidean distance (SED)* metrics [2]. It can count on both spatial and temporal aspects of a trajectory. For the calculations we assume that pedestrians move at constant speed on the experimental path. The ground truth path is divided evenly by the number of steps. Then we simply calculate the distance between a point on the ground truth and the corresponding point on the trajectory of interest.

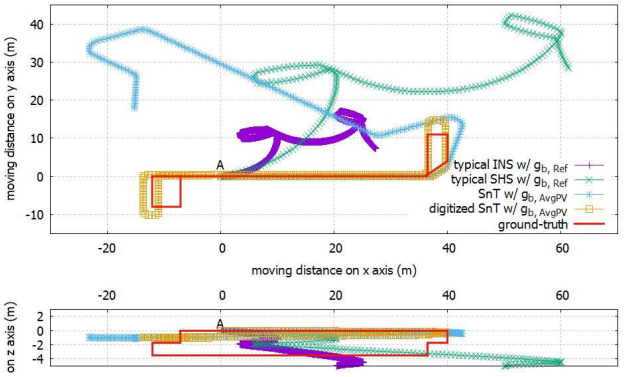

FIGURE 15. Pedestrian's trajectory on the xy-plane and the xz-plane of N-frame.

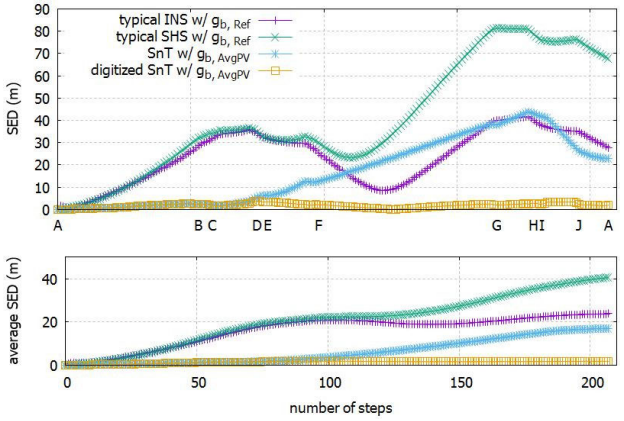

FIGURE 16. SED comparison of different pedestrian navigation schemes.

TABLE 1. A summary of performance comparison for different pedestrian navigation schemes.

	Typical INS w/ $\overrightarrow{g_{b,Ref}}$		Typical SHS w/ $\overrightarrow{g_{b,Ref}}$		SnT w/ $\overrightarrow{g_{b,AvgPV}}$		digitized SnT w/ $\overrightarrow{g_{b,AvgPV}}$	
	SED	average SED	SED	average SED	SED	average SED	SED	average SED
A	0.00	0.00	0.00	0.00	0.00	0.00	0.00	0.00
B	28.83	11.77	32.02	12.56	2.25	1.24	2.22	1.24
C	31.68	13.36	34.22	14.33	2.06	1.33	1.79	1.31
D	34.04	18.07	34.77	19.09	5.56	1.69	3.57	1.53
E	31.74	18.79	32.08	19.77	6.26	1.91	3.42	1.62
F	25.24	20.84	29.94	22.01	12.57	3.43	2.13	1.81
G	39.95	20.59	81.29	31.55	37.97	12.47	1.95	1.60
H	39.91	22.16	78.65	35.38	42.92	14.72	2.75	1.65
I	37.72	22.43	76.09	36.06	41.73	15.17	2.41	1.67
J	34.91	23.38	75.70	38.88	26.13	16.52	2.17	1.77
A	27.71	23.78	67.74	40.58	22.93	16.91	1.89	1.78

Figure 16 shows the SED comparison of different pedestrian navigation schemes on the horizontal plane and Table 1 provides a summary of the result. The upper graph of Figure 16 is SED for each step and the lower one is the average SED up to the step. The labels on the x-axis indicate the location of turns. We can see that the trajectory deviation of

typical INS and SHS increases rapidly from the early stage of walking. The SED decreases after passing point 'D' because the experimental path makes a complete loop returning to the starting point. Otherwise, it would keep diverging at a higher rate. We can see that the SED of SnT is suppressed until passing point 'C', but that the average SED diverges over time. It implies the importance of accurate estimation of heading change angles. The SED of digitized SnT is limited to a certain range. Most of the drifts result from the step length estimations of the Weinberg model we used. Large SED can be found around the landing of stairs: points 'D', 'E', 'H', and 'I'. A constant width of stair cannot be estimated by the model. The SED of digitized SnT at the final location is 1.89 m, which is about 1.2 % of the total length of the experimental path. By suppressing errors, even a pure inertial pedestrian navigation technique can be applied to mid-range navigations as well as short-range ones. We expect that, as a basic building block, the proposed ideas can play a role in inertial pedestrian navigation.

IV. CONCLUSION

Users' location is of vital importance having immense implications. Thanks to the technology of GNSS it becomes easier to get location data in outdoor environments. How-ever, people spend most of their time indoors, and providing indoor navigation and localization is a challenging task. In this paper, we presented two generic ideas for improving inertial pedestrian navigation. One is about estimation of gravitational acceleration in real-time. Since gravitational acceleration is dynamically estimated, for pedestrian navigation, we can determine moving distance and directional change without constraining the way of carrying a sensing device. The other is about digitization of heading change angles. By combining the estimated gravitational acceleration with a simple threshold-based turn detection algorithm we can practically digitize pedestrian's heading change angles. To demonstrate the effectiveness of the ideas a simple scheme, *steps-and-a-turn*, is designed by combining basic building blocks of inertial pedestrian navigation. From the experimental results with a complete daily route, we showed that the estimation of gravitational acceleration is consistent and robust, and that the digitization of heading change angles is highly effective in typical building environments. The positioning error of SnT scheme was about 1.2% of the total length of the experimental path, showing its applicability for mid-range navigations. We expect that many existing state-of-the-art schemes served on top of pure inertial pedestrian navigation will benefit from the proposed ideas. Sensor fusions or map-aided techniques using the proposed ideas in less restrictive experimental conditions will be pursued as future work.

APPENDIX

The personalized data of the four participants is provided for better understanding of the experiments in Section III.

TABLE 2. A summary of personalized data on participants.

participant	height (cm)	walking speed (#steps/sec)	k (the Weinberg model)
A	178.0	1.74	0.508
B	173.5	1.61	0.493
C	180.1	1.56	0.480
D	184.5	1.48	0.478

ACKNOWLEDGMENT

The author would like to thank Jeong Seol Son, Hyuck Yi, Jaewon Kim, and Hyunje Park for all their help with the data collections.

An earlier version of this paper was presented at the Seventh International Conference on Consumer Electronics Asia (ICCE-Asia) [DOI: 10.1109/ICCE-Asia57006.2022.9954745].

REFERENCES

[1] N. Zhu, J. Marais, D. Bétaille, and M. Berbineau, "GNSS position integrity in urban environments: A review of literature," *IEEE Trans. Intell. Transp. Syst.*, vol. 19, no. 9, pp. 2762–2778, Sep. 2018, doi: 10.1109/TITS.2017.2766768.

[2] J. Kim, "Feature-first add-on for trajectory simplification in lifelog applications," *Sensors*, vol. 20, no. 7, p. 1852, Mar. 2020, doi: 10.3390/s20071852.

[3] N. E. Klepeis, W. C. Nelson, W. R. Ott, J. P. Robinson, A. M. Tsang, P. Switzer, J. V. Behar, S. C. Hern, and W. H. Engelmann, "The national human activity pattern survey (NHAPS): A resource for assessing exposure to environmental pollutants," *J. Exposure Sci. Environ. Epidemiology*, vol. 11, no. 3, pp. 231–252, Jul. 2001, doi: 10.1038/sj.jea.7500165.

[4] R. Harle, "A survey of indoor inertial positioning systems for pedestrians," *IEEE Commun. Surveys Tuts.*, vol. 15, no. 3, pp. 1281–1293, 3rd Quart., 2013, doi: 10.1109/SURV.2012.121912.00075.

[5] H. Park, J. Noh, and S. Cho, "Three-dimensional positioning system using Bluetooth low-energy beacons," *Int. J. Distrib. Sensor Netw.*, vol. 12, no. 10, Oct. 2016, Art. no. 155014771667172, doi: 10.1177/1550147716671720.

[6] G. Li, E. Geng, Z. Ye, Y. Xu, J. Lin, and Y. Pang, "Indoor positioning algorithm based on the improved RSSI distance model," *Sensors*, vol. 18, no. 9, p. 2820, Aug. 2018, doi: 10.3390/s18092820.

[7] K. P. Subbu, B. Gozick, and R. Dantu, "LocateMe: Magnetic-fields-based indoor localization using smartphones," *ACM Trans. Intell. Syst. Technol.*, vol. 4, no. 4, pp. 1–27, Sep. 2013, doi: 10.1145/2508037.2508054.

[8] R. Faragher and R. Harle, "Location fingerprinting with Bluetooth low energy beacons," *IEEE J. Sel. Areas Commun.*, vol. 33, no. 11, pp. 2418–2428, Nov. 2015, doi: 10.1109/JSAC.2015.2430281.

[9] A. Soloviev. "Inertial error propagation: Understanding inertial behavior," Inside GNSS—Global Navigation Satellite Systems Engineering, Policy, and Design. Jun. 4, 2022. [Online]. Available: https://insidegnss.com/inertial-error-propagation-understanding-inertial-behavior/

[10] A. Manos, I. Klein, and T. Hazan, "Gravity-based methods for heading computation in pedestrian dead reckoning," *Sensors*, vol. 19, no. 5, p. 1170, Mar. 2019, doi: 10.3390/s19051170.

[11] A. Rehman, H. Shahid, M. A. Afzal, and H. M. A. Bhatti, "Accurate and direct GNSS/PDR integration using extended Kalman filter for pedestrian smartphone navigation," *Gyroscopy Navigat.*, vol. 11, no. 2, pp. 124–137, Apr. 2020, doi: 10.1134/S2075108720020054.

[12] (2022). *International Conference on Indoor Positioning and Indoor Navigation*. [Online]. Available: htpps://www.ipin-conference.org

[13] C. Yu, N. El-Sheimy, H. Lan, and Z. Liu, "Map-based indoor pedestrian navigation using an auxiliary particle filter," *Micromachines*, vol. 8, no. 7, p. 225, Jul. 2017, doi: 10.3390/mi8070225.
[14] J. J. Marron, M. A. Labrador, A. Menendez-Valle, D. Fernandez-Lanvin, and M. Gonzalez-Rodriguez, "Multi sensor system for pedestrian tracking and activity recognition in indoor environments," *Int. J. Ad Hoc Ubiquitous Comput.*, vol. 23, nos. 1–2, pp. 3–26, 2016, doi: 10.1504/IJAHUC.2016.078480.
[15] S. Y. Cho and C. G. Park, "MEMS based pedestrian navigation system," *J. Navigat.*, vol. 59, no. 1, pp. 135–153, Jan. 2006, doi: 10.1017/S0373463305003486.
[16] X. Ru, N. Gu, H. Shang, and H. Zhang, "MEMS inertial sensor calibration technology: Current status and future trends," *Micromachines*, vol. 13, no. 6, p. 879, May 2022, doi: 10.3390/mi13060879.
[17] J. Geng, L. Xia, J. Xia, Q. Li, H. Zhu, and Y. Cai, "Smartphone-based pedestrian dead reckoning for 3D indoor positioning," *Sensors*, vol. 21, no. 24, p. 8180, Dec. 2021, doi: 10.3390/s21248180.
[18] Z.-A. Deng, G. Wang, Y. Hu, and D. Wu, "Heading estimation for indoor pedestrian navigation using a smartphone in the pocket," *Sensors*, vol. 15, no. 9, pp. 21518–21536, Aug. 2015, doi: 10.3390/s150921518.
[19] D. Liu, L. Pei, J. Qian, L. Wang, P. Liu, Z. Dong, S. Xie, and W. Wei, "A novel heading estimation algorithm for pedestrian using a smartphone without attitude constraints," in *Proc. Int. Conf. Ubiquitous Positioning, Indoor Navigat. Location Based Services*, Shanghai, Nov. 2016, pp. 29–37, doi: 10.1109/UPINLBS.2016.7809947.
[20] D. M. Henderson, "Euler angles, quaternions, and transformation matrices," Nat. Aeronaut. Space Admin., Mission Planning Anal. Division, Washington, DC, USA, Contractor Rep. NASA-CR-151435, 1977. [Online]. Available: https://ntrs.nasa.gov/citations/19770019231
[21] X. Niu, Q. Wang, Y. Li, Q. Li, and J. Liu, "Using inertial sensors in smartphones for curriculum experiments of inertial navigation technology," *Educ. Sci.*, vol. 5, no. 1, pp. 26–46, Mar. 2015, doi: 10.3390/educsci5010026.
[22] D. A. Winter, "Kinematic and kinetic patterns in human gait: Variability and compensating effects," *Human Movement Sci.*, vol. 3, nos. 1–2, pp. 51–76, Mar. 1984.
[23] C. Huang, F. Zhang, Z. Xu, and J. Wei, "Adaptive pedestrian stride estimation for localization: From multi-gait perspective," *Sensors*, vol. 22, no. 8, p. 2840, Apr. 2022, doi: 10.3390/s22082840.
[24] C. Soaz and K. Diepold, "Step detection and parameterization for gait assessment using a single waist-worn accelerometer," *IEEE Trans. Biomed. Eng.*, vol. 63, no. 5, pp. 933–942, May 2016, doi: 10.1109/TBME.2015.2480296.
[25] D. Trong Bui, N. Nguyen, and G.-M. Jeong, "A robust step detection algorithm and walking distance estimation based on daily wrist activity recognition using a smart band," *Sensors*, vol. 18, no. 7, p. 2034, Jun. 2018, doi: 10.3390/s18072034.
[26] M. Vezočnik, R. Kamnik, and M. B. Juric, "Inertial sensor-based step length estimation model by means of principal component analysis," *Sensors*, vol. 21, no. 10, p. 3527, 2021, doi: 10.3390/s21103527.
[27] H. Weinberg, "Using the ADXL202 in pedometer and personal navigation applications," Analog Devices, Wilmington, MA, USA, Application Notes AN-602, vol. 2, 2002, pp. 1–6.
[28] J. Diebel, "Representing attitude: Euler angles, unit quaternions, and rotation vectors," *Matrix*, vol. 58, nos. 15–16, pp. 1–35, 2006.
[29] D. Pavllo, C. Feichtenhofer, M. Auli, and D. Grangier, "Modeling human motion with quaternion-based neural networks," *Int. J. Comput. Vis.*, vol. 128, no. 4, pp. 855–872, Apr. 2020, doi: 10.1007/s11263-019-01245-6.
[30] STMicroelectronics. (2013). *LSM303D—Ultra-Compact High-Performance eCompass Module: 3D Accelerometer and 3D Magnetometer*. [Online]. Available: https://www.st.com/en/mems-and-sensors/lsm303d.html
[31] STMicroelectronics. (2013). *L3GD20—MEMS Motion Sensor: Three-Axis Digital Output Gyroscope*. [Online]. Available: https://www.st.com/en/mems-and-sensors/l3gd20.html
[32] T. Pachi and A. Ji, "Frequency and velocity of people walking," *Struct. Eng.*, vol. 83, no. 3, pp. 36–40, 2005. [Online]. Available: https://www.researchgate.net/publication/291793625_Frequency_and_velocity_of_people_walking

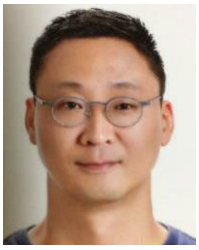

JUNSEONG KIM (Member, IEEE) received the B.S. and M.S. degrees in electronics engineering from Chung-Ang University, Seoul, South Korea, and the Ph.D. degree in electrical engineering from the University of Minnesota, Minneapolis. He is currently a Professor with the School of Electrical and Electronics Engineering, Chung-Ang University. Previously, he was a Research Assistant with the Minnesota Supercomputing Institute, University of Minnesota, and a Senior Design Engineer with Intel Corporation, Portland, OR, USA. His research interests include computer architecture, high-performance computing, embedded system design, IoT and lifelog, and location-based services.